# Crab Cavity Instabilities Due to Fundamental Crabbing Mode and Crab Cavity Impedance

A Senior Project

By

Trevor Loe

Advisor, Dr. Themis Mastoridis

Department of Physics, California Polytechnic University SLO

June 8, 2023

Approval Page

**Title: Crab Cavity Instabilities Due to Fundamental Crabbing Mode and Crab Cavity Impedance**

**Author: Trevor Loe**

**Date Submitted: June 7, 2023**

Senior Project Advisor: Dr. Themis Mastoridis

Signature

Date

# Contents

# List of Tables



# List of Figures

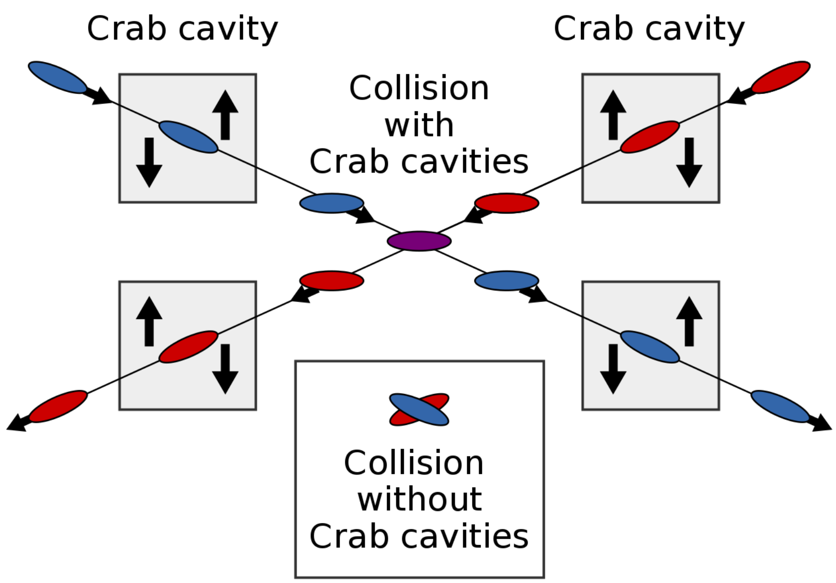


Figure 1: Diagram depicting how crab cavities alter the beam collision at the interaction point. Note that the relative scale of ovals is off compared with the EIC bunches. If a single bunch was as thick as a pencil, it would be 10m long. Image taken from [2].

# 1 Introduction

The collision rate is an important parameter for particle accelerators, since a higher rate shortens the time to discoveries. New technologies are required to significantly increase the collision rate in new and updated accelerators. One such technology is crab cavities. Both the High-Luminosity Large Hadron Collider (HL-LHC) and the Electron Ion Collider (EIC) will implement them. The specifications for their EIC implementation can be found in [1].

Crab cavities are electromagnetic cavities with a resonant frequency in the RF part of the spectrum. Their purpose is to apply a tilt to the beam as it approaches its collision point. The beam will move sideways (like a crab), leading to a better overlap at the interaction point. A visual diagram of this can be seen in figure 1. This must be done just before the interaction point. Afterwards, the beam must be uncrabbed to return to its original orientation. Their effective use can increase luminosity by an order of magnitude [3].

To give the beam the desired kick, the cavity's voltage is oscillated at a high frequency (in the RF spectrum), on the order of hundreds of MHz. Since the oscillation of the cavity voltage will go through many cycles as the beam completes one turn, the beam can take advantage of this by organizing the particles into small packets, called RF bunches. The oscillation is timed so the beam coming through will get a voltage centered around the zero crossing of the sine wave. This way, the beam centroid is unaffected, whereas the head and tail receive kicks with opposite signs, leading to the bunch rotation. If the bunch is much smaller than the RF period, then to good approximation the voltage around the zero crossing is linear. This gives a uniform tilt of the beam.

Due to the micrometer and nanosecond precision that these cavities must operate at, their voltage magnitude and phase must be heavily regulated to ensure efficient operation. Cavity regulation is carried out through the low-level radio frequency (LLRF) system. Careful design of this system is tantamount to the cavities' success.

The first use of crab cavities in a circular accelerator was in the KEKB accelerator in Japan in 2007. The cavities achieved marginal success, largely due to operational complexities.

The EIC will employ crab cavities to adjust the beam tilt by 25 mrad at the interaction point. This will happen for both the electron storage ring (ESR) and hadron storage ring (HSR). For both rings, there are two sets of crabbing and uncrabbing cavities: 8 cavities operating at 197 MHz and 4 cavities operating at 394 MHz. This is to account for the fact that the beam is too long to get a linear kick from the 197 MHz cavity. The front and tail of the beam extend slightly into the nonlinear region of the sinusoidal voltage oscillation. The 394 MHz cavity is placed to reduce this nonlinearity, giving the beam a more uniform kick [1].

# 2 Motivation

The EIC LLRF system has 3 main functions: to keep RF noise minimized, to regulate the crabbing and uncrabbing voltages (while keeping their sum at 0), and to reduce the crab cavity impedance to prevent transverse instabilities.

## 2.1 Control Architecture

To accomplish this, the LLRF system will implement a high-bandwidth proportional controller and a low bandwidth integral controller. The high-bandwidth controller will respond to higher frequency changes, within a turn, while the low-bandwidth controller acts as a low-pass filter. This will respond to changes in the system on the order of many turns and will maintain the DC value of the voltage constant. Because of the slow response time of the integral controller, the proportional controller is mainly determining the system stability, both in transient beam loading and in impedance reduction. Thus, the proportional controller parameters are mainly studied.

Dependent on more precise LLRF requirements, an additional one-turn feedback (OTFB) controller and/or global controller will be implemented. The OTFB controller has high gain on very close to the frequency of the revolution harmonics and very low gain elsewhere to increase impedance reduction at those frequencies without reducing the RF loop stability margins. It resembles an inverted comb filter. The quadrupole, sextupole and octupole magnets used in any particle accelerator for focusing can only focus in one direction, while defocusing in the other. This means that the beam will get narrower in the x-direction, while getting wider in the y-direction. The magnets are always placed in a pattern of x-focusing followed by y-focusing to keep both directions well managed. The repeated focusing and defocusing of the beam in either of the transverse directions gives rise to an oscillation of beam about it's ideal transverse position at a known frequency, called the betatron frequency. The frequency is specified by the betatron tune, given by $\nu_b = f_b/f_{rev}$, the ratio of the betatron frequency to the revolution frequency. For the EIC, the betatron frequency is $\sim 0.22$. The OTFB controller must take this into account by placing its notches at the revolution harmonics $\pm f_b$. Each revolution harmonic will then have two notches for the upper and lower betatron frequency offset, called the betatron sidebands.

An additional controller, known as the global controller has also been studied for its use in the EIC. The global controller is an independent controller that samples the sum of the crabbing and uncrabbing voltage and acts on the crabbing cavity. It is a low-bandwidth integral controller, which accordingly acts over the time-scale of many accelerator turns. The lower bandwidth is chosen as to avoid interaction with the main LLRF controllers and create an unwanted feedback loop. Its main purpose is to act in the case of a cavity loss, in order to control the other cavity before the beam is dumped.

### 2.2 RF noise reduction

The transverse emittance is the area of the beam's phase-space and quantifies the bunch's transverse size. The control system inevitably injects noise into the system, causing the emittance of the beam to grow over time, characterized by the emittance growth rate [4]. In the case of the ESR, the synchrotron radiation produced by the acceleration of charged particles (the electrons) counteracts this emittance growth.

For the HSR, the situation is more difficult. Intrabeam scattering (IBS) creates an additional source of emittance growth along with that produced by RF noise. On top of that, the synchtrotron radiation damping time is extremely slow. To counteract both these effects, a hadron cooling system is implemented. This cooling system is already designed to counter the effects of IBS, so it is important to ensure that the emittance growth created by the RF noise is not too high [5].

### 2.3 Voltage Regulation

The beam tilt and transverse position are given by the equations

$$\frac{\Delta\theta}{2} = \frac{2\pi f_{cc}\Delta A\sqrt{\beta_{cc}\beta^*}}{cE_b} \tag{1}$$

$$x = \frac{c}{2\pi f_{cc}}\tan\left(\frac{\theta}{2}\right)\Delta\phi \tag{2}$$

From equation 1 the beam tilt is directly proportional to the voltage amplitude deviation ($\Delta A$). From equation 2 the transverse position is directly proportional to the voltage phase deviation ($\Delta\phi$). Thus to maintain a proper beam tilt of 25 mrad and reasonable transverse position, the voltage amplitude and phase must be precisely regulated.

The beam's electromagnetic field will disturb the cavity each time the beam passes through, known as transient beam loading. This disturbance can be modelled, treating the cavity as an LRC circuit. The disturbance, seen by the cavity each time the beam passes through, is proportional to the transverse position offset, $\Delta x$. There are other controllers around the loop that will reduce $\Delta x$ after the uncrabbing cavity, but if the offset is greater than those controllers can respond to, there could a runaway effect as $\Delta x$ grows with $\Delta\phi$. Therefore an important metric in studying the transient beam loading is whether the transverse position offset deviate beyond the threshold for which the other controllers around the loop can manage it.

Along with the disturbances created by beam loading, the LLRF system must respond to noise in the transverse position. This is caused from noise in the beam sampling (quantization error is the dominant effect here) and error in the placement of the cavity in the beamline, inducing a constant transverse position error. This effect is similar to that of the accelerating system, but with some small differences described in [6].

### 2.4 Impedance Reduction

As a charged particle passes through the crab cavity, it creates a "wake field", an electromagnetic field disturbance following the particle. These wake fields will then go on to affect the next particle in the bunch, leading to a further field disturbance. These are known as couple-bunch instabilities and are described in [7].

Viewing this in the frequency domain, certain modes of bunch motion will be excited by these accumulating wake fields, and may cause the cavity voltage to grow over time. Because the strength of these wake fields is determined by the beam current (as having more particles in the beam would inevitably create more wake fields), this can be thought of as more complex case of Ohm's law,

$$V_{wake} = I_b Z_{cav}$$

Where $V_{wake}$ is the wake field voltage, $I$ is the beam current and $Z_{cav}$ is the transverse impedance, capturing cavity's interaction with the beam that excites these modes. This impedance is determined both by the cavity and the controller parameters and will generally be frequency dependent.

If the wake fields are too powerful, they will strongly couple the motion of different bunches. If the growth rate due to the wake field interactions is greater than the natural decay rate of the unperturbed beam, the beam will become unstable. Because the beam current is directly related to the number of collisions and thus the data collected, it is externally set. Thus, to reduce these wake field interactions and improve the stability of our system, we must reduce the impedance $Z_{cav}$.

Each of these requirements for the control system impose restrictions and trade-offs on the controller parameters. It is expected and has already been found in [8] that these trade-offs will lead to conflicting optimizations for the controller parameters. The EIC is still being designed, so it is early to optimize the controller parameters. Still, understanding these trade-offs may be important in making decisions about the design of other accelerator components. Thus, this work is more focused on obtaining qualitative relationships between the parameters and the controller requirements, as well as informing other design aspects for the EIC that must be determined sooner (such as transverse position noise thresholds).

# 3 Previous Work

## 3.1 RF Noise Reduction Study

The transverse emittance growth rate can be determined from the following equations, taken from [5]

$$\left(\frac{\epsilon_{x,y}}{dt}\right)_{\Delta\phi} = \frac{1}{N_{cav}\beta^*}\left[\left(\frac{ec\theta_{cc}f_{rev}}{4\omega_{RF}}\right)^2\right] C_{\Delta\phi}(\sigma_\phi)\frac{2\sigma^2_{\Delta\phi}}{f_{rev}} \tag{3}$$

$$\left(\frac{\epsilon_{x,y}}{dt}\right)_{\Delta A} = \frac{1}{N_{cav}\beta^*}\left[\left(\frac{ec\theta_{cc}f_{rev}}{4\omega_{RF}}\right)^2\right] C_{\Delta A}(\sigma_\phi)\frac{4\sigma^2_{\Delta A}}{f_{rev}} \tag{4}$$

These give us the transverse emittance growth rate (in x or y) due to phase noise ($\Delta\phi$) or amplitude noise ($\Delta A$). Here $N_{cav}$ is the number of cavities, $\beta^*$ is the beta function at the interaction point, $c$ is the speed of light, $e$ is the charge of an electron, $\theta_{cc}$ is the crabbing angle (25 mrad in our case), $\sigma_\phi$ is the RMS bunch length, $f_{rev}$ is the revolution frequency (78 kHz in our case), $\omega_{RF}$ is the cavity RF frequency, $\sigma^2_{\Delta\phi}$ and $\sigma^2_{\Delta A}$ are the phase and amplitude noise powers sampled by the beam. The term $C_{\Delta\phi}(\sigma_\phi)$ or $C_{\Delta A}(\sigma_\phi)$ are functions of the bunch length $\sigma_\phi$ and show the scaling of the phase noise or amplitude noise effects with the bunch length. Using equations 3 and 4, one can obtain a target noise power threshold based off a target emittance growth rate. Using a target emittance growth rate of 1%/hr, the target noise power for different operational modes of the EIC can be seen in table 1.

The noise power thresholds given for all the energies of the HSR are below the threshold of current electronic technology. Thus, the crab cavity RF noise level cannot be maintained at an

| Mode | $\sigma_{\Delta\phi}$[$\mu$rad] | $\sigma_{\Delta A}$[1e-6] |
|---|---|---|
| ESR 5 GeV | 805 | 12700 |
| ESR 10 GeV | 860 | 13600 |
| ESR 18 GeV | 548 | 7060 |
| HSR 41 GeV | 3.09 | 10.1 |
| HSR 100 GeV | 2.69 | 9.36 |
| HSR 275 GeV | 1.75 | 7.07 |

Table 1: Target noise threshold for different energy levels of the EIC. Values are taken from [5].

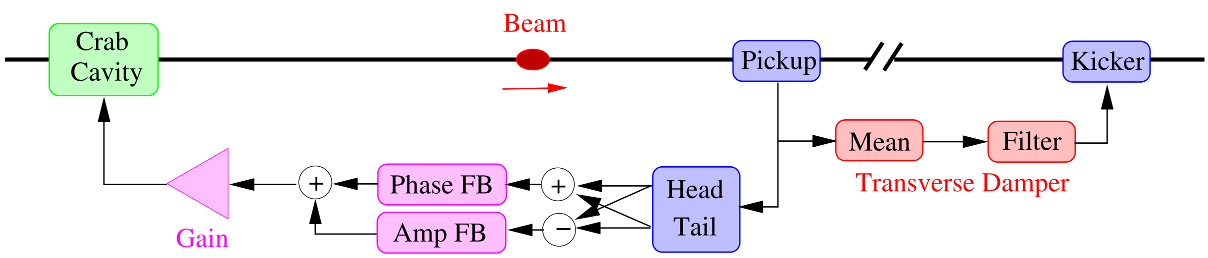


Figure 2: Proposed crab cavity RF noise feedback system. Taken from [5].

allowable level without additional controllers. One such controller was designed and studied in simulation. The system would involve sampling the head and tail bunch position, using those to estimate the bunch tilt and offset and adjusting the crab cavity current accordingly.

The proposed RF noise feedback system can be seen in figure 2. The system was studied for it's effect on the transverse emittance growth rate, both in the system's gain and delay. As expected, the emittance growth rate decreases with increased system gain both from the amplitude noise and phase noise. The system was found to be less effective as the tune spread was increased. With the addition of measurement noise, a loss in the system's effectiveness at higher gains was seen. This is expected as the higher gains will greatly amplify measurement noise and that effect will eventually overpower the benefit of the increased gain. Thus, there is a local minimum in the emittance growth rate where below such a minimum, the growth rate is dominated by the crab cavity RF noise and above such a minimum, the growth rate is dominated by the measurement noise. This is seen in figure 3.

The nature of the measurement noise and the system's sensitivity to it will depend highly on the pickup location and specifications. As such, the placement and specifications of the pickup should be carefully quantified. The LLRF system design will greatly affect the noise that is

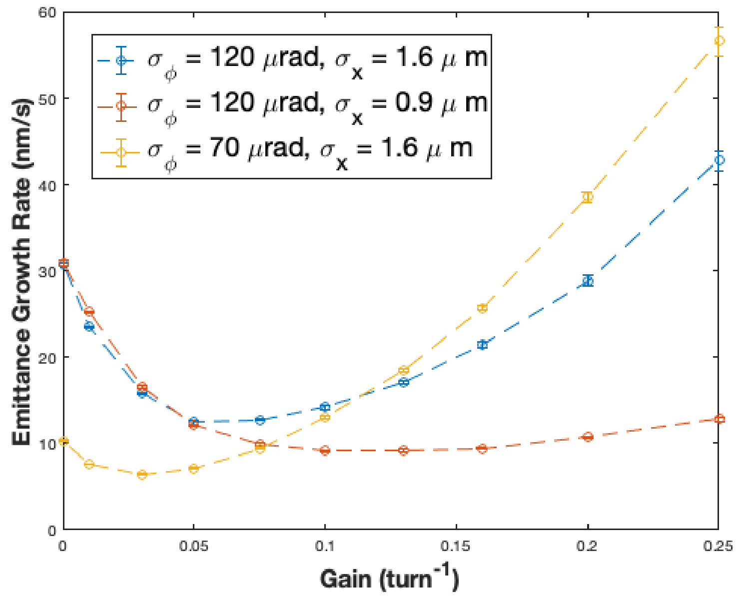


Figure 3: Transverse emittance growth rates plotted against the RF noise feedback gain in the presence of measurement noise. 3 different RF and measurement noise levels are shown. Taken from [5].

amplified and reducing the LLRF bandwidth will generally lower the noise that is integrated. To meet such small noise thresholds for the HSR, the LLRF bandwidth should be lowered as much as possible.

### 3.2 Transient Beam Loading Study

A simulation was developed and tested to test the effect of the controller parameters on the controller's voltage regulation ability. The simulation considered 2 cavities, one crabbing and one uncrabbing (although the effect of multiple cavities can be seen by scaling the transmitter current) and their interaction with a the beam. It was implemented in MATLAB and Simulink, based on a different simulations used to understand the transient beam loading the accelerating cavities. The transient beam loading was modeled via the equations in [9]. More specifically, the transmitted and reflected beam current through the crab cavity was modelled as

$$J_g = \left[\frac{V_\perp}{2(R/Q)_\perp}\left(\frac{1}{Q_{ext}} + \frac{1}{Q_0}\right) + \frac{x\omega}{c} I_{b,DC} F_b \sin(\phi)\right] + i\left[\frac{x\omega}{c} I_{b,DC} F_b \cos(\phi)\right] \tag{5}$$

$$J_r = \left[\frac{V_\perp}{2(R/Q)_\perp}\left(\frac{1}{Q_{ext}} - \frac{1}{Q_0}\right) - \frac{x\omega}{c} I_{b,DC} F_b \sin(\phi)\right] - i\left[\frac{x\omega}{c} I_{b,DC} F_b \cos(\phi)\right] \tag{6}$$

Where $V_\perp$ is the cavity voltage (in general, time dependent), $Q_{ext}$ and $Q_0$ are the cavity and external quality factors, $(R/Q)_\perp$ is the ratio of the cavity resistance to it's quality factor, $\omega$ and $c$ are constants of the cavity operation, and $x$ is the transverse position deviation. In the system $x$ is related to the cavity phase via equation 2. It can be seen from equations 5 and 6 that the transmitted current phase will never be nonzero if the x-position is nonzero. So if the transverse position deviation starts at 0, it will remain at 0. Because of this, the initial $x$ offset was important for studying the controller parameters. The two cases tested were that of a constant initial $x$ offset of 0.6mm and several levels of injected Gaussian noise in the $x$ offset values. In both cases, the proportional controller gain was adjusted and its effect on the systems transients recorded.

From figure 4, 5, and 7 the transient in the voltage and the transverse position is increased as the gain is decreased, as expected. Even in the worse cases, the transients were not at concerning levels (several kV for the voltage, several $\mu$m for $x_{IP}$, and several tens of nm for $x_{\text{offset}}$). The transient power seen in figure 6 is a significant increase from the nominal value, but is not concerning for the system operation. However, it must be taken into account for the transmitter specifications.

The effect of the OTFB controller was also studied for its effects on the system's transients, yielding a significant increase in beam performance.

The OTFB gives us a significant improvement in the transverse position and transmitter power usage. The OTFB cutoff frequency was studied but the effects on the voltage transients were found to be negligible. Since the transients seen in the studies of the controller parameters

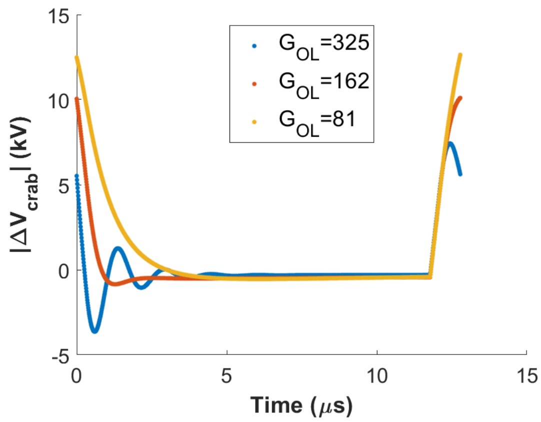


Figure 4: Deviation in crabbing cavity voltage magnitude from nominal value over one turn for 3 different proportional gain values. Data was taken using a constant initial $x$ offset of 0.6mm. Taken from [6].

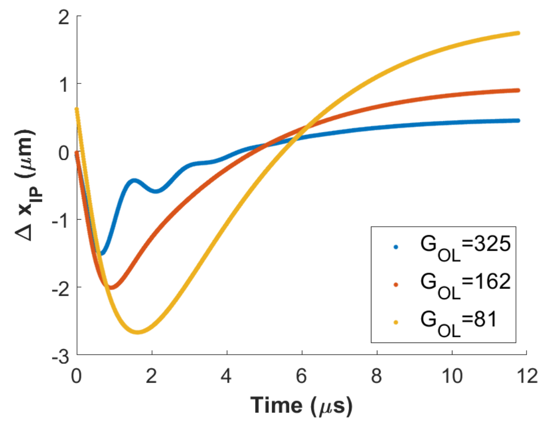


Figure 5: Deviation in transverse beam position over a turn for 3 different proportional gain values. Beam position $x_{\mathrm{IP}}$, is measured after the crabbing cavity but before the uncrabbing. Data was taken using a constant initial $x$ offset of 0.6mm. Taken from [6].

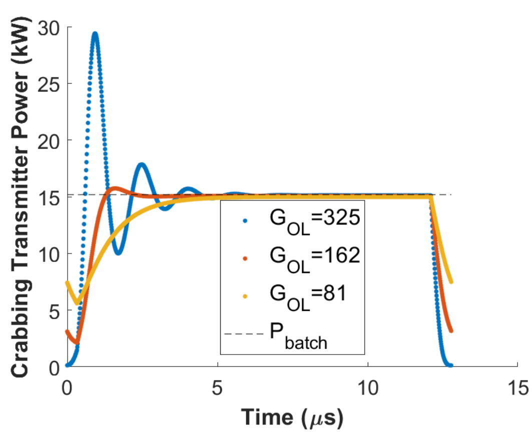


Figure 6: Transmitter power usage over a turn for 3 different proportional gain values. Data was taken using a constant initial $x$ offset of 0.6mm. Taken from [6].

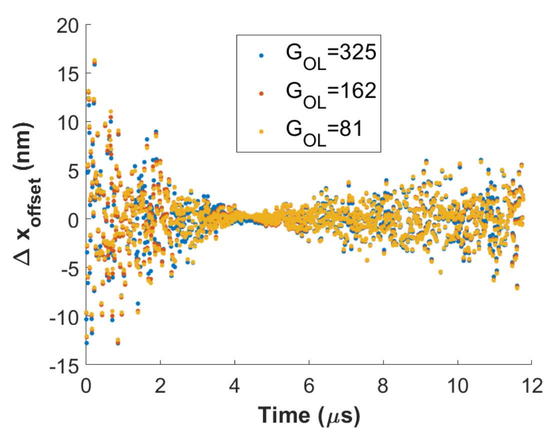


Figure 7: Deviation in transverse beam position over a turn for 3 different proportional gain values. Beam position, $x_{\mathrm{offset}}$, is measured after the uncrabbing cavity. Data was taken using injected Gaussian noise in the $x$ offset with an rms value of 100$\mu$m.

are not concerning in any case, the decision of whether to implement the OTFB will depend more on the requirements given by the RF noise reduction and the transverse impedance reduction.

Additionally, the effect of the global controller was studied for it's ability to bring the cavity voltage down in the case of a cavity loss. These studies and further discussion can be found in [6].

# 4 Mathematical Formulations

## 4.1 Cavity Impedance

As described above, particles moving through the cavity field will produce a wake field, affecting future particles. The evolution of these wake-fields in time must be regulated for the beam to remain stable. Viewing this system in the frequency domain, we can consider the transfer function

$$Z(\omega) = \frac{V_{wf}(\omega)}{I_{beam}(\omega)} \tag{7}$$

where $V_{wf}$ is the voltage produced by the wake fields and $I_{beam}$ is the beam current. So understanding the beam's stability in the frequency domain is closely tied with understanding the system's impedance.

The cavities impedance can be simply modeled as an RLC circuit with a transfer function given by

$$H_{cav}(\omega) = \frac{\omega_r R_x}{\omega(1 + jQ_l(\omega_r/\omega - \omega/\omega_r))} \tag{8}$$

also taken from [7] where $R_x$ is the transverse impedance, $\omega_{ri}$ is the resonant frequency of the cavity and $Q_l$ is the loaded quality factor for the cavity. This gives us the open loop impedance for the cavity with no feedback. As seen in equation 8, this impedance grows asymptotically as $\omega \to \omega_r$. For our beam system described by equation this would mean unbound growth for the bunch phase and instability for the beam.

To reduce the impedance at this point, we implement a feedback controller given by the open loop transfer function

$$H_{fb}(\omega) = G_{fb} e^{-j(\delta * \omega + \phi)} \tag{9}$$

where $\delta$ is the loop delay, $\phi$ is the loop phase error and $G_{fb}$ is the feedback gain.

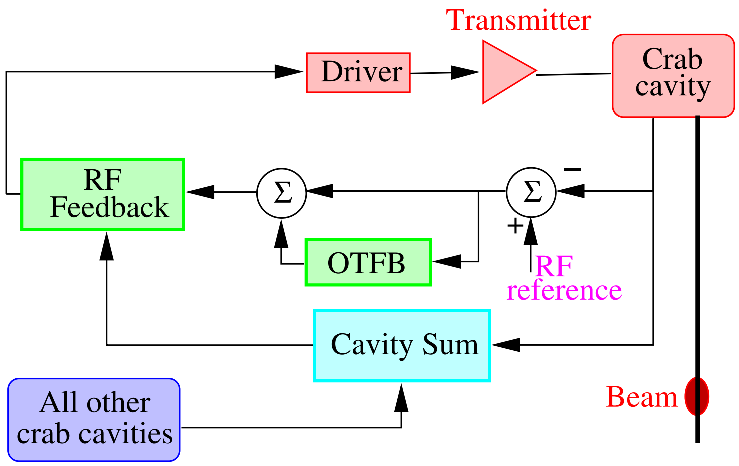


Figure 8: Block diagram depicting RF feedback and OTFB and their interaction within the system.

From figure 8 the relationships between the cavity voltage, control current and beam current can be seen in terms of the transfer functions as

$$I_{control} = V_{cav} H_{fb}$$
$$V_{cav} = H_{cav}(I_{beam} + I_{control}) = H_{cav} I_{beam} + H_{cav} H_{fb} V_{cav}$$
$$V_{cav}(1 - H_{fb} H_{cav}) = H_{cav} I_{beam}$$

Then the impedance is given by

$$\frac{V_{cav}}{I_{beam}} = Z = \frac{H_{cav}}{1 - H_{fb} H_{cav}} \tag{10}$$

The OTFB has a more complicated open-loop transfer function found in [10], $H_{comb}$ to achieve the desired frequency response (a spike at the betatron sidebands of every revolution harmonic). Because of its different interaction with the cavity, seen in figure 8 above, the OTFB controller yields a closed loop transfer function for the impedance given by

$$Z = \frac{H_{cav}}{1 - H_{fb} H_{cav}(1 + H_{comb})} \tag{11}$$

This will yield not only a reduction in the fundamental resonance of the cavity, but a reduction at each of the betatron sidebands of each revolution harmonic.

## 4.2 Stability of Beam

Given a certain system transfer function, $G(s)$ and controller transfer function, the closed loop transfer function $H(s)$ is given by

$$H(s) = \frac{G(s)}{1 + GH(s)}$$

$H(s)$ will go unstable at it's poles, when $1 + GH(s) = 0$. We can say that our system is stable if it's pole will never be hit for any frequency $\omega$. This means that our system is stable if the function $1 + GH(s)$ has no zeros. Defining $G_o(s) = GH(s)$ we can use Cauchy's argument principle to find any zeros.

Cauchy's argument principle states that for a contour in the complex plane, $\gamma$ encompassing $P$ poles and $Z$ zeros of a complex function $f(z)$, the contour $f(\gamma)$ will encircle the origin $P - Z$ times. If we consider the following contour $\gamma$:

- Travelling from $-Rj$ to $Rj$ along the imaginary axis
- Travelling in a semicircular arc encompassing part of the right-half plane from $Rj$ back down to $-Rj$

then as we let $R \to \infty$, the contour gamma will encompass the entire right-half plane. So the contour $G_o(\gamma)$ will circle the origin $P - Z$ times, where $P$ is the number of poles of $G_o$ in the right-half plane and $Z$ is the number of zeros of $G_o$ in the right-half plane. Because we care about the zeros of the function $1 + G_o(s)$, we consider the number of times $G_o(\gamma)$ encircles $-1$. Thus, we can say that the contour $G_o(\gamma)$ will encircle $-1$ clockwise $n_c + n_o$ times where $n_c$ is the number of poles of the closed-loop system and $n_o$ is the number of poles of the open loop system.

In our case, our open loop system has no poles in the right-half plane (due to feedback), so the transformation of our nyquist contour $G_o(\gamma)$ will encircle the point $-1$ clockwise exactly $n_c$ times, indicating the number of closed loop poles our system has in the right-half plane. Because our system is asymptotically stable, the portion of the nyquist contour travelling in a semi-circular arc has a negligible effect as we increase $R$. So we only consider the contour generated from pluggin in all $j\omega$, where $\omega$ runs over all possible frequencies. In practice only a limited range of frequencies are considered, as our system attenuates sufficiently for high frequencies. So our system will be stable if this contour does not encircle $-1$.

To account for the coupled bunch instabilities, we must consider a slightly different situation. To do this, we obtain an equation of motion from the beam over time by examining the coherent force on the particles, given by

$$F_x(\theta, t) = i\frac{q^2\omega_0}{2\pi R}\sum_{k=-\infty}^{\infty}(D_k Z_x(k) + d_k)e^{i(kM+s)(\theta-\omega_0 t)-i\Omega t} \tag{12}$$

Here $\frac{q^2\omega_0}{2\pi R}$ is a constant related to the accelerator's design, $s$ is the coupled bunch mode being considered, $\omega_0$ is the RF angular frequency, $M$ is the number of bunches, $\Omega$ is the betatron frequency, and $Z_x(k)$ is the transverse impedance (impedance for the cavity's transverse voltage in the x-direction), evaluated at $(kM + s + \nu_b)\omega_0 + \Omega$, the $k$'th mode of the cavity's operating frequency plus a shift due to the betatron tune. Here $D_k$ is the $k$'th Fourier component of the particles' dipole magnetic moment.

A full derivation of the stability method can be found in [11] (although for a slightly different system). The derivation goes on to obtain a matrix equation for the system's frequency response in terms of the external drive $d_k$ by considering only finitely many $k$ values. The $K$ matrix generated will satisfy the equation

$$\mathbf{d} = \mathbf{D} - K(\Omega)\mathbf{D} = (\mathbf{1} - K(\Omega))\mathbf{D} \tag{13}$$

where $\mathbf{d}$ is the vector for the external drive, and $K(\Omega)$ is a matrix, where $K_{k,m}$ is proportional to the transverse impedance, $Z_x(k)$ and the DC beam current (the number of particles going through the cavity per second multiplied by the charge of a single particle, $q$). Since $d_k$ is the $k$th mode of the system's drive in frequency space, it can be thought of as the system frequency response for a particular mode. The equation can be loosely thought of as the unperturbed beam dipoles (represented by the $\mathbf{1}$) on the right side, minus the perturbation due to beam particles interacting with the cavity and each other via the wake fields. This interaction is encompassed in $K(\Omega)$ for a finite number of modes considered. When $K(\Omega)$ is small, the drive is just the unperturbed beam, and the system is stable. As $K(\Omega)$ grows, the contribution from the coupling of the beam particles via the wake field interactions eventually becomes greater than the unperturbed beam. This crossover point is when $\det(\mathbf{1} - K(\Omega)) = 0$.

Similar to a system's transfer function, $\mathrm{Re}(\det(\mathbf{1} - K(\Omega)))$ gives an estimate for the negative of the growth rate over all nodes (since it is the natural dipole decay rate given by $\mathbf{D}$ minus the growth rate given by $K(\Omega)\mathbf{D}$ and $\mathrm{Im}(\det(\mathbf{1} - K(\Omega)))$ is an estimate for the system's oscillation frequency. Similar to the nyquist criterion described above, the system will be stable if the the complex contour given by $\det(\mathbf{1} - K(\Omega))$ as a parameterized curve in $\Omega$ does not encircle the origin so the system will have no modes with a positive growth rate.

# 5 Simulation Description

The simulation consists of the interfacing of two models: one written by Dr. Mastoridis to accurately model the crab cavity and controller impedance, and one written by Mike Blaskiewicz at Brookhaven National Laboratory calculating the generalized nyquist criterion to determine the beam's stability.

## 5.1 Impedance generation

Implemented in MATLAB, the impedance is calculated in accordance to the formulation described in section 4.1. In the accelerator the cavities operate at a much higher frequency than the revolution harmonics (197 MHz vs. 78 kHz). The controllers' input signal is demodulated against the cavity's operating frequency and the controllers' output signal is then modulated against the cavity's operating frequency. This allows us to design the controllers' frequency response around 0 Hz rather than 197 MHz. Thus all frequency responses are reported centered around zero. A frequency range of $\pm 5MHz$ was chosen for study as it both encompasses many revolution harmonics and extends to significant impedance fall-off. This justification can be seen in figure 9.

The cavity's impedance is calculated according to equation 8. Then from equations 10 and 11, the closed loop impedances are calculated, centered about zero. The difference impedances can be seen in figure 9.

The simulation also allows us to check the stability of the system based on the frequency

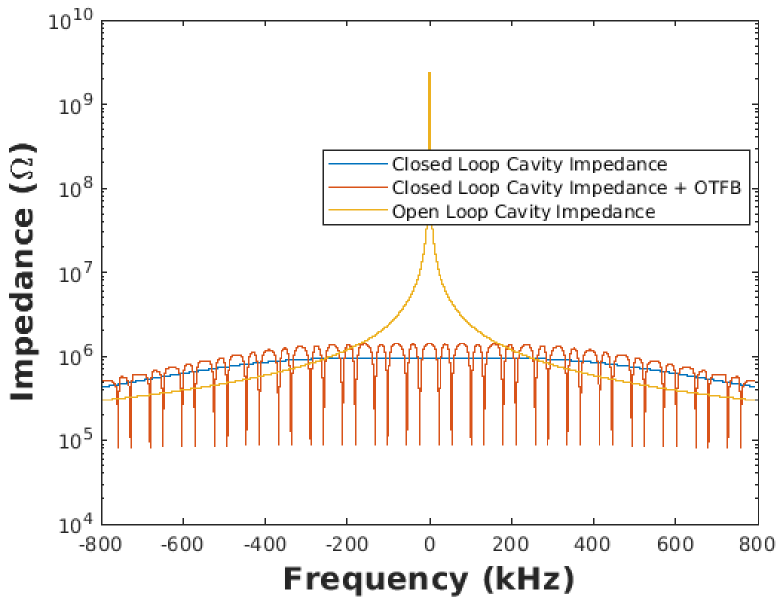


Figure 9: Impedance for the open loop cavity, closed loop with proportional feedback controller, and closed loop with OTFB controller shown over the selected frequency range. The fundamental resonance is reduced by several orders of magnitude by the feedback controller and the betatron sidebands are reduced by an order of magntiude by the OTFB.

response of the cavity with the controllers. This is done using the nyquist criterion (described in section 4.2). This is done by examining the transfer function between the beam's output current and the beam's input current in a loop (different than the transfer function considered in equation 7). An example of such a nyquist plot can be seen in figure 10.

The accelerator will have two sets of cavities: 8 cavities operating at 197 MHz and 4 cavities operating at 394 MHz. Since these cavities are operating in series, their respective impedances can be calculated separately and added together to get the total impedance.

## 5.2 Stability Determination

Taking in the impedance generated from the first code described in section 5.1, the second code, implemented in fortran, computes the determinant of $\mathbf{1} - K$ in equation 13 to get the system's complex frequency response for each evaluation frequency, $\Omega$. The set of frequencies at which to evaluate $K$ is the same as the frequencies used to evaluate $Z(\omega)$ (described in section 5.1). Since the impedance is given in a discrete array, the values are interpolated at frequencies not

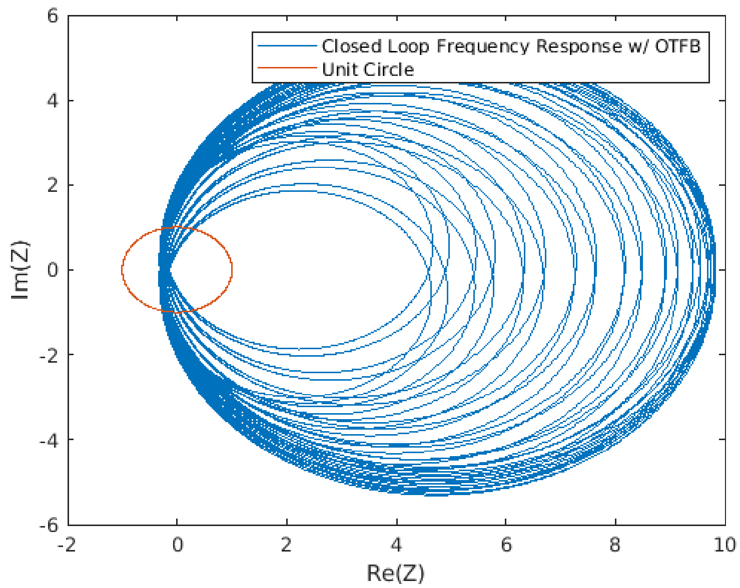


Figure 10: Nyquist plot generated from cavity, feedback and OTFB response. Here the contour does not encircle $-1$, so the loop is stable by this metric.

given in the impedance array. As such, it is important to choose a frequency step size small enough to capture the fast-changing behavior of the OTFB, seen in figure 9.

Similar approximations to [11] are made with regard to the truncation of the vectors in equation 13. Only 3 positive and 3 negative frequency modes are considered (as the system's closed loop bandwidth is expected to fall off dramatically after this point).

Plotting the frequency response given by $\det(\mathbf{1} - K(\Omega))$ over all evaluation frequencies as a complex contour allows us to see the nyquist criterion for the system (described in section 4.2). Assuming our system has no open-loop poles in the right-half plane for any mode, we know that the system will be stable if the contour generated does not encircle the point 0. A sample nyquist plot generated from this code can be seen in figure 11.

Since the frequency response of the system increases with the DC beam current, decreasing the DC beam current will shrink the contour generated. Thus, any controller will be stable if the DC current is lowered enough. The main metric we are concerned with is the maximum allowed DC current, as it is proportional to the maximum number of particles in the accelerator. By lowering the DC current until the nyquist plot generated is stable, we can determine the

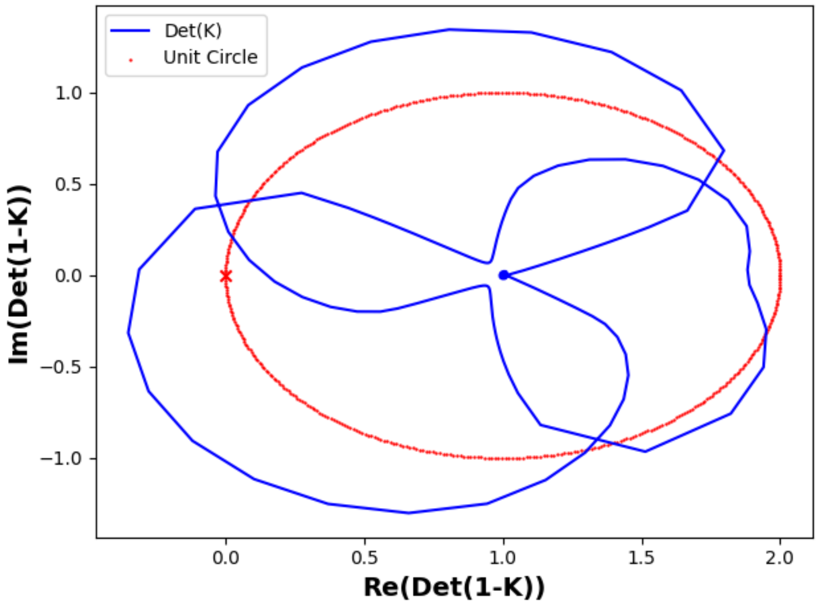


Figure 11: A nyquist plot generated by the simulation using the impedance generated from the code described in section 5.1. Here it is clear that the system is unstable because the contour encircles the point 0 (marked with a red $\times$). Also plotted is the unit circle to give an estimate of the phase and gain margins.

maximum allowed DC current, effectively measuring how stable the system is with the given controller architecture.

# 6 Results

The controller parameters studied included the feedback gain ($G_{fb}$ above), the feedback phase ($\phi$ in equation 9), the OTFB gain and the OTFB phase. For each parameter, the value was varied over an operationally reasonable range, and the effect on the max current was observed. As such, the edge values for each parameter actually correspond to an unstable or marginally stable control loop. The maximum allowed currents with nominal controller parameters are shown in table 2. The studies on the feedback controller parameters are shown in tables 3 and 4. The studies on the main OTFB system parameters are shown in tables 5 and 6.

In table 2, we can see that the addition of the OTFB on top of the RF feedback gives us a significant increase in the maximum allowed current of a factor of $\sim$ 40. Although the

| Case | No OTFB | OTFB | OTFB upper sideband | OTFB lower sideband | OTFB both cavities |
|---|---|---|---|---|---|
| $I_{b,max}$ | 1.3 | 50.5 | 0.05 | 5.5 | 33.6 |

Table 2: $I_{b,max}$ for different baseline cases with nominal controller parameters. In all cases, the RF feedback is on with a gain of 2500 and a phase deviation of 0°. In all cases with OTFB, the gain is set to 10 and the phase is set to 0.

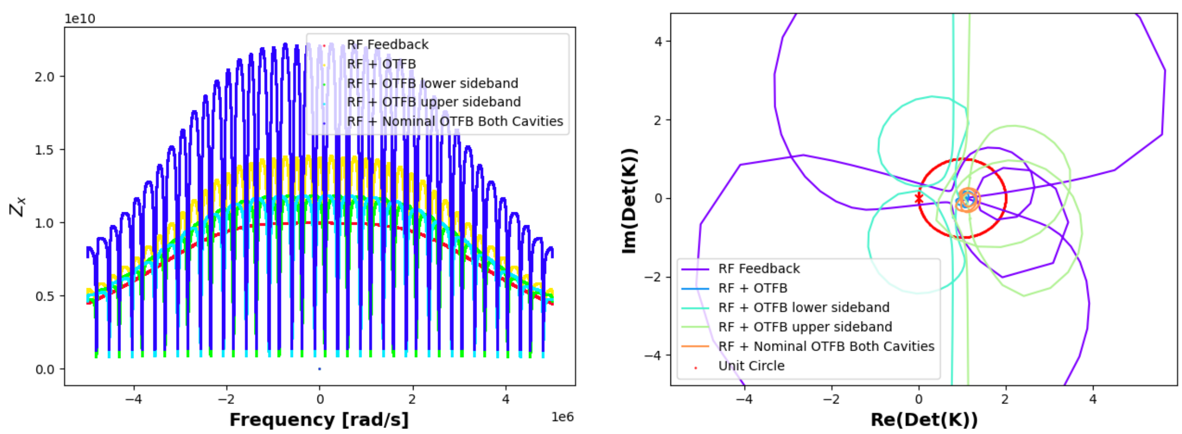


(a) (b)

Figure 12: Impedance (a) and nyquist plot (b) for all the baseline cases overlaid. In the nyquist plots the case of RF feedback with OTFB is small enough to not be visible. The cases of the upper and lower sidebands have parts of their nyquist plots cut off, as the most prominent lobes were too big to show with the other cases. But it can be seen that the case of the upper sideband is encircling 0, where the case of the lower sideband is not. All cases were run with a current of 3.5 A.

impedance at the betatron sidebands of the revolution harmonic is reduced by only a factor of 10, the system's response is expected to depend on both the growth rate, which is proportional to the impedance at the betatron sidebands, and the tune shift. It is expected that the addition of the OTFB reduces both. The dependence of the stability of this system due to the tune shift is still being investigated. As expected, the addition of the 4 cavities operating at 394 MHz reduces the maximum allowed current by a factor of $\sim 1.5$. This is because the additional cavities increase the impedance by a factor of $\sim 1.5$. Since the growth rate should be proportional to $Z_x((kM+s+\nu_b)\omega_0)-Z_x((kM+s-\nu_b)\omega_0)$, it is expected that including only the upper sideband on the OTFB (the $+\nu_b$) would significantly reduce the stability of the system while including on the lower sideband (the $-\nu_b$) would increase the stability of the system. Instead, both of these cases are worse than the nominal OTFB, at different degrees. We suspect this is because the asymmetric OTFB changes *both* growth rates and tune shifts. This will be investigated in future work. These cases can also been seen in figure 12.

| Gain | 1000 | 2000 | 2500 | 3000 | 4000 |
|---|---|---|---|---|---|
| $I_{b,max}$ | 20.7 | 41.2 | 50.5 | 61.6 | 81.7 |

Table 3: $I_{b,max}$ with RF feedback gain.

| Phase(°) | -15 | -10 | -5 | 0 | 5 | 10 | 15 |
|---|---|---|---|---|---|---|---|
| $I_{b,max}$ | 2.6 | 5.6 | 23.4 | 50.5 | 32.0 | 14.2 | 7.5 |

Table 4: $I_{b,max}$ with RF feedback phase.

| Gain | 1 | 5 | 10 | 15 | 20 | 30 |
|---|---|---|---|---|---|---|
| $I_{b,max}$ | 9.3 | 27.8 | 50.5 | 75.8 | 61.6 | 11.4 |

Table 5: $I_{b,max}$ with OTFB gain.

| Phase(°) | -15 | -10 | -5 | 0 | 5 | 10 | 15 |
|---|---|---|---|---|---|---|---|
| $I_{b,max}$ | 3.0 | 8.6 | 27.9 | 50.5 | 35.3 | 17.1 | 9.5 |

Table 6: $I_{b,max}$ with OTFB phase.

From the studies of the feedback controller parameters we determine two relationships. From table 3 we see that the maximum current increases with the feedback gain proportionally (if we

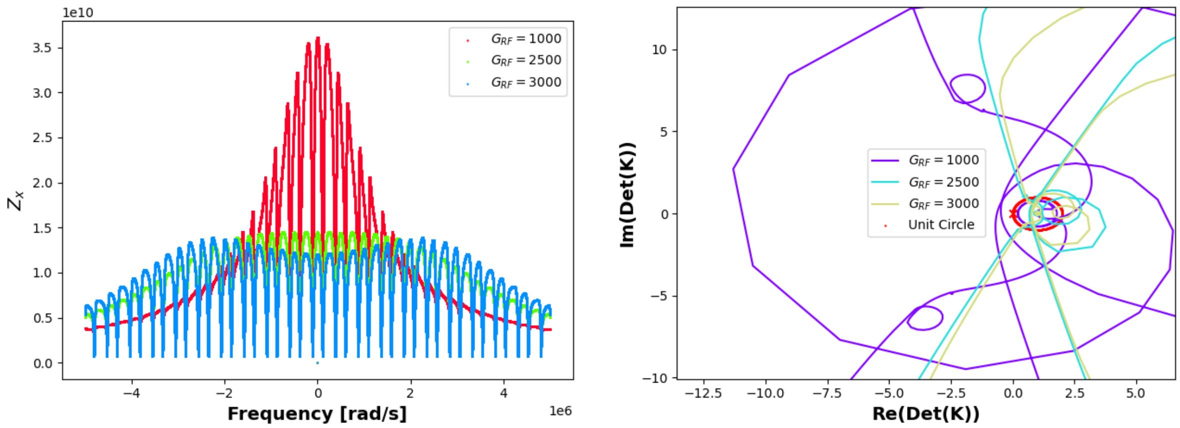


(a) (b)

Figure 13: Impedance (a) and nyquist plot (b) for several cases of varying the RF gain. In all cases, some of the larger stable modes are cutoff to better view the point at the origin. For these cases the current was kept at 40 A, and no other controller parameters were changed from their nominal value.

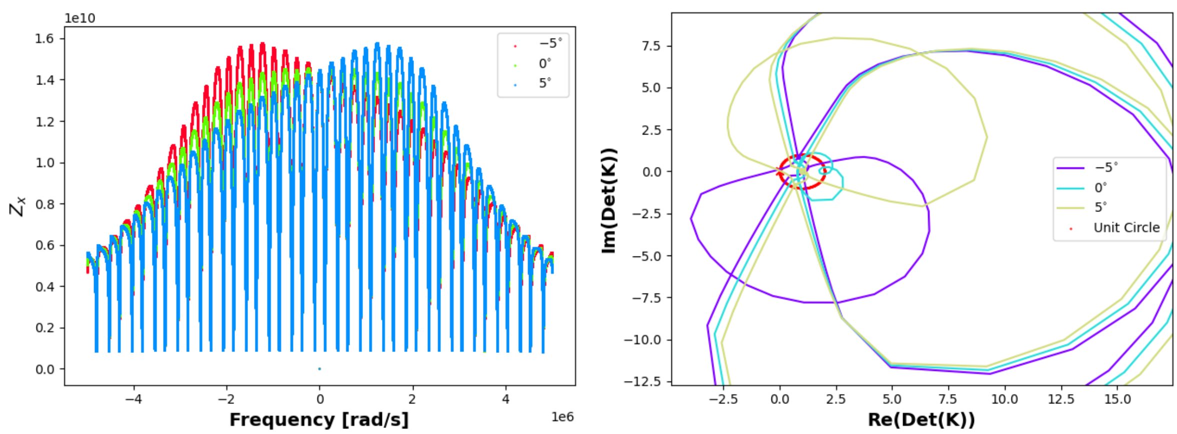


(a) (b)

Figure 14: Impedance (a) and nyquist plot (b) for several cases of varying the RF phase. For these cases the current was kept at 30 A, and no other controller parameters were changed from their nominal value.

double the gain, we see roughly a doubling of the max DC current). This is telling to the fact that the system stability only depends on the first 3 or 4 modes. Only the impedance at those modes will decrease inversely proportional with the RF gain. This can be seen in figure 13a. Since the frequency response (in the $K$ matrix of equation 13) is roughly proportional to both

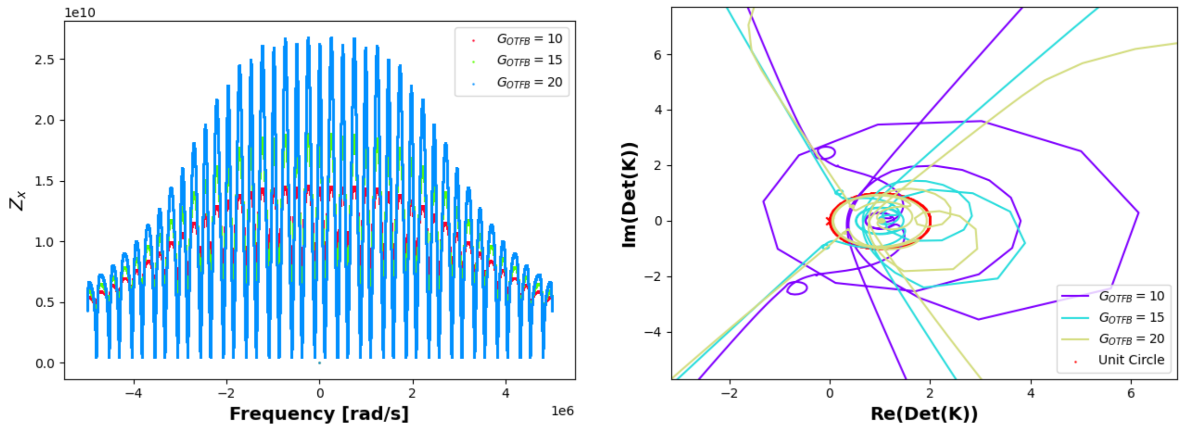


(a) (b)

Figure 15: Impedance (a) and nyquist plot (b) for several cases of varying the OTFB gain. In all cases, some of the larger stable modes are cutoff to better view the point at the origin. For these cases the current was kept at 60 A, and no other controller parameters were changed from their nominal value.

the DC current and the impedance this would suggest that the stability of the system only seems to depend on the impedance that is changing linearly with the gain, the first 3 or so modes. The linear change in the systems response with the gain can be seen in figure 13b. Increases in the feedback gain decrease the loop stability. From table 4 we see that both positive and negative phase rotations decrease the transverse stability, shown by a lower DC current. Deviations from 0 phase generally decrease the loop stability as well.

The OTFB controller parameters study showed two more trends. From table 5 we see that the maximum current increases roughly proportionally with the OTFB gain up to a gain of about 15. After this point there seems to be a local maximum in $I_{b,max}$ after which the max DC current drops dramatically. This is unexpected behavior as increases in the OTFB gain correspond to a decrease in the system impedance at the betatron sidebands of the revolution harmonics. Since the stability of the system should only depend on the impedance sampled at these frequencies (see equation 12), a decrease in the impedance at those frequencies should be beneficial for the system's stability. An explanation for the maximum in $I_{b,max}$ is the fact that the OTFB notches become narrower as the gain is increased. After a certain point, the notch is so narrow that the tune spread (the spread in betatron frequency over the different bunches) is

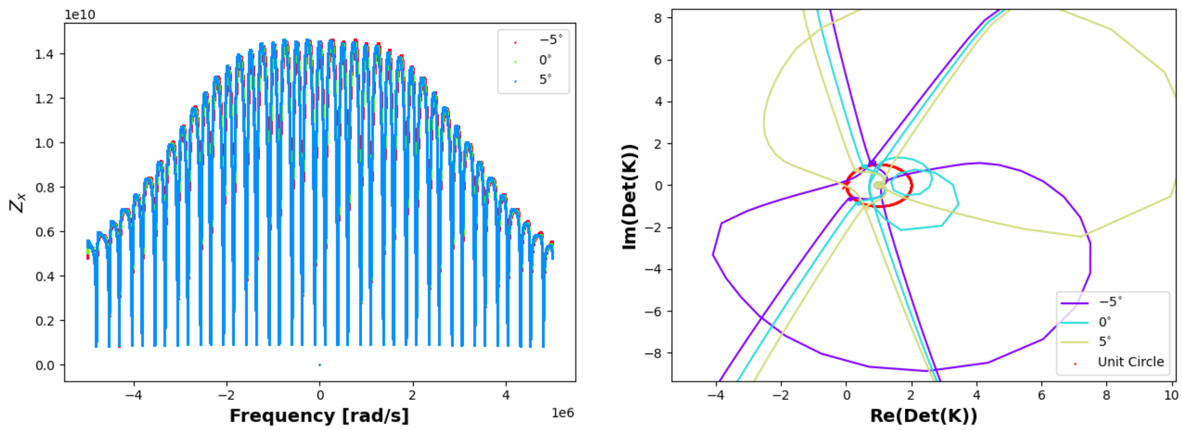


(a) (b)

Figure 16: Impedance (a) and nyquist plot (b) for several cases of varying the OFTB phase. For these cases the current was kept at 37 A, and no other controller parameters were changed from their nominal value.

greater than the width of the OTFB notch so many of the beam particles have a betatron shift putting them outside the notch from the OTFB. These particles would then see a much higher impedance and the OTFB would not be effective for them. We speculate that above a gain of about 15, this effect overpowers the effect of the reduced gain, leading to a net loss in stability. The narrowing of the OTFB notches can be seen in figure 17.

The OTFB phase showed a similar trend to the feedback phase in that both positive and negative phase deviations resulted in a decrease in the maximum DC current. There was also a similar asymmetry in that the positive phase rotations were slightly more stable than the negative ones. Both positive and negative phase deviations lead to decreased loop stability.

# 7 Conclusions and Future Work

Our most important conclusions from the study are those seen in tables 2-6. The most significant effect seen is that of changing either the RF or OTFB phase. Changing the gains generally produced a proportional change in $I_{b,max}$, except for the specific case of the OTFB discussed above. The expected beam current for the EIC is 2.5 amps for the ESR and 1 amp for the HSR, much lower than any of the maxima found at nominal operation. The trends from this study

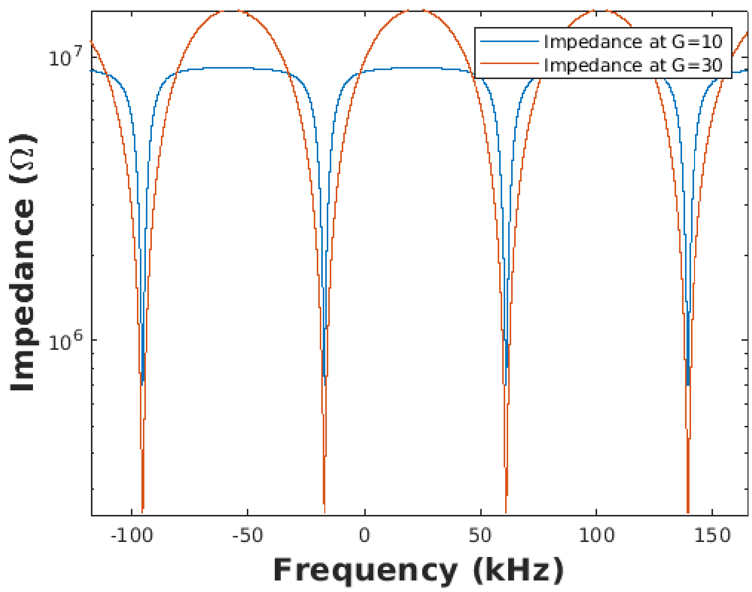


Figure 17: Impedance of closed loop system with different OTFB gains. As the gain is increased, the width of individual notches gets narrower.

give us an idea of how far from the nominal operation the controller parameters can go keeping us above this expected current. This is especially important in the case of the RF gain, as the nominal gain of 2500 might not be feasible for the EIC.

Many of these trends give demands on the controller parameters that are conflicting with the results of [6] and [5]. Most concerning of these conflicts is the demand of [5] to lower the RF feedback bandwidth, which may require a lower RF gain. Lowering the RF gain would likely produce a similar decrease in the maximum stable beam current, which could drop us below the expected EIC beam current. It may also be possible to lower the RF feedback bandwidth without decreasing the gain, as the system's stability seems to be dependent on only the first 3 or 4 modes (see discussion above in section 6). A choice must be made for each of the controller parameters (especially the RF and OTFB gains) that balances the demands of the RF noise with the impedance reduction presented here.

As more machine parameters become clearer and fully determined, the accuracy of this simulation can be increased and its use, alongside other simulations of the EIC crab cavities will be useful tools in designing the LLRF system.

## 8 Acknowledgements

The author would like to, above all, thank Dr. Mastoridis for the mentorship, impromptu control theory and accelerator physics lectures, patience, and general support throughout the research. The author would like to thank Mike Blaskiewicz for allowing us to use his simulation. The author would also like to thank Trevor Hidalgo and Matti Toivola for their great work as fellow research students on parts of the previous work, and Siddhi Upadhyaya for her support and interesting conversations throughout the research and for assistance in editing this manuscript.

## References

[1] F. Willeke and J. Beebe-Wang, "Electron ion collider conceptual design report 2021," Feb. 2021. DOI: 10.2172/1765663. [Online]. Available: https://www.osti.gov/biblio/1765663.

[2] I. Raynova, *Crab cavities: Colliding protons head-on*, Dec. 2017. [Online]. Available: https://web.archive.org/web/20190613132152/https://home.cern/news/news/accelerators/crab-cavities-colliding-protons-head.

[3] R. Calaga, "Crab cavities for the lhc upgrade," *Proceedings of Chamonix 2012 workshop on LHC Performance, February 2012*, [Online]. Available: http://cds.cern.ch/record/1493034.

[4] P. Baudrenghien and T. Mastoridis, "Transverse emittance growth due to rf noise in the high-luminosity lhc crab cavities," *Phys. Rev. ST Accel. Beams*, vol. 18, p. 101 001, 10 Oct. 2015. DOI: 10.1103/PhysRevSTAB.18.101001. [Online]. Available: http://link.aps.org/doi/10.1103/PhysRevSTAB.18.101001.

[5] K. Smith, T. Mastoridis, P. Fuller, P. Mahri, and Y. Matsumura, "Eic transverse emittance growth due to crab cavity rf noise: Estimates and mitigation," Feb. 2022. DOI: 10.2172/1846026. [Online]. Available: https://www.osti.gov/biblio/1846026.

[6] T. Mastoridis, K. Smith, T. Hidalgo, T. Loe, and M. Toivola, "Time-domain simulation of the crab cavity/beam interaction," Brookhaven National Laboratory, Tech. Rep. BNL-224087-2023-TECH, Feb. 2023. [Online]. Available: https://technotes.bnl.gov/Home/ViewTechNote/224087?selectedPageNumber=0.

[7] K.-Y. Ng, "Physics of collective beam instabilities," Aug. 2000. [Online]. Available: https://www.osti.gov/biblio/760458.

[8] C. Rivetta, T. Mastorides, J. D. Fox, D. Teytelman, and D. Van Winkle, "Modeling and simulation of longitudinal dynamics for low energy ring–high energy ring at the positron-electron project," *Phys. Rev. ST Accel. Beams*, vol. 10, p. 022 801, 2 Feb. 2007. DOI: 10.1103/PhysRevSTAB.10.022801. [Online]. Available: https://link.aps.org/doi/10.1103/PhysRevSTAB.10.022801.

[9] J. Tückmantel, "Cavity-Beam-Transmitter Interaction Formula Collection with Derivation," Tech. Rep. CERN-ATS-Note-2011-002 TECH, Oct. 2010. [Online]. Available: `http://cds.cern.ch/record/1323893`.

[10] P. Baudrenghien, T. Mastoridis, and J. Molendijk, "The LHC One-Turn Feedback," 2012. [Online]. Available: `https://cds.cern.ch/record/1424396`.

[11] M. Blaskiewicz, "Landau damping with high frequency impedance," in *Particle accelerator. Proceedings, 23rd Conference, PAC'09, Vancouver, Canada, May 4-8, 2009*, M. Comyn, S. Koscielniak, V. R. W. Schaa, and P. W. Schmor, Eds., JACoW: Geneva, Switzerland, Dec. 2010, pp. 4592–4594.